



# Selective electro-oxidation of glycerol to tartronate or mesoxalate on Au nanoparticle catalyst via electrode potential tuning in anion-exchange membrane electro-catalytic flow reactor

Zhiyong Zhang<sup>a</sup>, Le Xin<sup>a</sup>, Ji Qi<sup>a</sup>, David J. Chadderdon<sup>a</sup>, Kai Sun<sup>b</sup>,  
Kayla M. Warsko<sup>a</sup>, Wenzhen Li<sup>a,\*</sup>

<sup>a</sup> Department of Chemical Engineering, Michigan Technological University, 1400 Townsend Drive, Houghton, MI, 49931, United States

<sup>b</sup> Department of Materials Science and Engineering, University of Michigan, Ann Arbor, MI, 48190, United States



## ARTICLE INFO

### Article history:

Received 24 May 2013

Received in revised form

16 September 2013

Accepted 2 October 2013

Available online 16 October 2013

### Keywords:

Glycerol

Electro-catalysis

Gold nanoparticles

Green chemical production

Selective oxidation

## ABSTRACT

A potential-controlled glycerol oxidation to tartronate or mesoxalate was demonstrated on Au nanoparticle catalysts in a self-designed anion-exchange membrane electro-catalytic flow reactor. The investigation clearly shows that by tuning the anode potential from 0.35 to 0.65 V, the selectivity to tartronate dropped from 79% to 26%, while that to mesoxalate increased from 0% to 57%. The tests also indicate that the elongation of reaction time will only increase the glycerol conversion, having little effects on the product distribution. The work may open a new route for the controllable oxidation of biorenewable polyols to valuable chemicals.

© 2013 Elsevier B.V. All rights reserved.

## 1. Introduction

The exploration of sustainable and cost-effective catalytic processes for production of valuable chemicals from biologically derived compounds is in urgent need to replace petrochemical feedstocks [1–6]. However, the complexity of these multi-functionalized structures leads to difficulty limiting oxidation or reduction to the target functional group without affecting the rest. Glycerol is a simple polyol that is massively produced from biodiesel manufacturing, and is considered an ideal biorenewable feedstock for the production of a series of high value oxygenated chemicals [7–14]. On monometallic Pt, Pd, and Au catalysts, it is easy to oxidize one of the primary-OH group, achieving high yield of glycerate (or glyceric acid in low pH aqueous solution) [10,15,16], but further oxidation of another primary -OH, and further the secondary -OH group to obtain tartronate and mesoxalate is far less efficient, due to the over-competition from C-C bond cleavage (yielding glycolate or oxalate). Reasonable selectivities to tartronate and mesoxalate from heterogeneous chemical oxidation of glycerol were obtained under restricted conditions either through low efficient multi-step sequential batch reactions [17,18]

or on complicated multi-metallic catalysts (Ce-Bi-Pt-Pd/C [19] or Ce-Bi-Pt/C [17]); however, it is still unclear what is the dominant factor governing the oxidation of different functional groups. As a result, it is still hard to achieve controlled oxidation of different -OH groups or breakage of C-C bond in glycerol oxidation.

Besides heterogeneous catalysis, electro-catalytic oxidation of glycerol has been investigated, heavily focused on the voltammetries combined with spectroscopies or chromatographies in half-cells [14,20–24]. Seminal work has been done by Koper et al. [14,24] through combining the in-situ sample collection ex-situ HPLC analysis technique with linear scan voltammetries, and they successfully captured the products generated on Pt and Au polycrystalline electrodes under a wide range of potentials. Although these fundamental works from Koper et al. demonstrated that the electrode potential can serve as a facile and controlled driven force instead of molecule O<sub>2</sub> or H<sub>2</sub>O<sub>2</sub> for the chemical oxidation of glycerol, the products are mainly glycerate and glycolate. No tartronate and mesoxalate were detected on Au, and only trace amount of tartronate was detected on Pt [14,24]. The glycerol electro-oxidation on bimetallic PtBi, PdBi and trimetallic PtPdBi catalysts were also investigated in alkaline electrolyte by Simoes et al. [21,25]. Based on the HPLC analyses after long-term chronoamperometries, at 50% glycerol conversion, the authors detected glycerate and tartronate at 0.55 V, and mesoxalate at 0.85 V, but no product selectivity was reported in their work. Meanwhile, with the

\* Corresponding author. Tel.: +1 906 487 2298; fax: +1 906 487 3213.

E-mail addresses: [wzli@mtu.edu](mailto:wzli@mtu.edu), [liwenzhen@gmail.com](mailto:liwenzhen@gmail.com) (W. Li).

assistance of in-situ FTIR techniques, Simoes et al. observed the formation hydroxypyruvate on Au nanoparticles at potentials >0.7 V [20], which is proposed to be an intermediate to mesoxalate [25]. However, weak signals of tartronate and mesoxalate were probed only at very high potentials (>1.2 V vs. RHE) on an Au electrode surface [26]. These results seem to have closed the door to a fine electrochemical manipulation of the glycerol oxidation to deeper-oxidized valuable tartronate ( $1564 \text{ US\$ g}^{-1}$ ) and mesoxalate ( $156 \text{ US\$ g}^{-1}$ ) [7].

Recently, our group successfully demonstrated that glycerol can be electro-oxidized to tartronate and mesoxalate with simultaneous generation of electric power under anion-exchange membrane fuel cell (AEMFC) working conditions [27,28]. The massive production of tartronate and mesoxalate from electro-oxidation of glycerol also indicated that the carbon cloth based porous electrodes may function differently from glycerol electro-oxidation in a half cell setting (with smooth glassy carbon electrode). Using a similar testing configuration, Vizza et al. also observed the formation of tartronate from glycerol on Pd-based catalysts under a galvanostatic condition [29,30], which further supported that a porous electrode will facilitate the generation of deeper-oxidized products. However, in their works, no mesoxalate was observed, and the controlling factor in glycerol electro-oxidation process remains unclear. On the Au/C nanocatalyst, we recently observed the anode potential can be a key factor determining the degree of glycerol oxidation [28]. However, due to the lack of direct anode potential control, we could not obtain high yield of tartronate without the formation of mesoxalate under AEMFC test conditions.

In order to confirm the predominant effect of anode potential over glycerol oxidation, to distinguish the potential requirement for the generation of tartronate or mesoxalate, and to achieve high yield to tartronate or mesoxalate, in this work, an efficient potential controlled electro-catalytic process was successfully demonstrated on a supported Au nanoparticle (Au/C) catalyst in a delicately-designed anion-exchange membrane electro-catalytic flow reactor. By tuning the anode applied potential, glycerol can be selectively converted to tartronate or mesoxalate, with a switch potential of 0.45 V (vs. Reversible Hydrogen Electrode (RHE)). At an anode potential of 0.4 V and 50 °C, a selectivity of 78% to tartronate was obtained (at a glycerol conversion of 35%) and no mesoxalate was detected; while at 0.65 V, the main product was switched to mesoxalate (55% selectivity at a glycerol conversion of 78%).

## 2. Experimental

### 2.1. Chemicals

$\text{AuCl}_3$  was purchased from Alfa Aesar.  $\text{LiBEt}_3\text{H}$  (1 M in THF) and 1-octadecene were purchased from Acros Organics. Oleylamine was purchased from Aldrich Chemistry. Glycerol (99.8%) was purchased from Fisher Chemical. Carbon cloth (untreated) was purchased from Fuel Cell Store. FAA anion-exchange membrane (110  $\mu\text{m}$ ) was purchased from FumA-Tech. Prior to testing, the FAA anion-exchange membrane was treated as recommended by the manufacturer.

### 2.2. Synthesis of Au/C catalysts

The preparation of 40 wt% Au/C catalyst was reported in our previous publications [31,32]. Briefly, 151.7 mg of  $\text{AuCl}_3$  was dissolved in a mixture of 16 ml of octadecene and 4 ml of oleylamine under nitrogen gas flow. The system was then heated to 80 °C, followed by a quick injection of 1.5 ml of  $\text{LiBEt}_3\text{H}$ . After holding the temperature constant for 10 min, the Au nanoparticles (NPs) were obtained

after quickly cooling down the solution to room temperature and separated by centrifugation. The as-prepared Au-NPs were then dispersed into 50 ml of hexane and slowly dropped into an ethanol dispersion of carbon black (148.0 mg). The final product Au/C catalyst (40 wt%) was obtained after filtration and washed with copious ethanol.

### 2.3. Physical characterizations

The X-ray diffraction (XRD) analysis of the Au/C catalyst was carried out on a Scintag XDS-2000 diffractometer with a  $\text{Cu K}\alpha$  source ( $\lambda=1.5406 \text{ \AA}$ ). The transmission electron microscopy (TEM) image of Au/C was collected on JEOL JEM-4000FX with an operating voltage of 200 kV. High resolution TEM (HR-TEM) was performed by JEOL 2010F with the operating voltage of 300 kV.

### 2.4. Single electro-catalytic flow reactor setup and potential controlled glycerol electro-oxidation

The potential controlled electro-oxidation of glycerol was investigated in a self-designed electro-catalytic flow reactor ( $5.0 \text{ cm}^2$  active cross-sectional area). A Au/C based anode ( $5.0 \text{ mg}_{\text{Au}} \text{ cm}^{-2}$ ) and a Pt/C based cathode ( $1.0 \text{ mg}_{\text{Pt}} \text{ cm}^{-2}$ ) were firstly prepared by airbrushing on carbon cloth (PTFE-untreated, 381  $\mu\text{m}$ , Fuel Cell Store) that serves as the liquid diffusion layers (LDL), and assembled with a solid anion-exchange membrane (FAA, 110  $\mu\text{m}$ , Fuma-Tech), home-made anode graphite block with serpentine flow pattern and high-density polyethylene cathode chamber. The system was sealed with the assistance of unreactive silicon gaskets (508  $\mu\text{m}$ , Fuel Cell Store) and a torque of 20 N m. During each run, 8.0 ml of glycerol + KOH solution was introduced into a plastic vessel and pumped into the anode at the rate of  $1.0 \text{ ml min}^{-1}$  through a closed loop by a peristaltic pump (Gilson Minipuls 3), while a KOH solution (the same pH as the anode reactant solution) was cycled through the cathode chamber. The anode applied potential was controlled by potentiostats (Versastat, Princeton Applied Research) through a  $\text{Hg/HgO}/1.0 \text{ M KOH}$  electrode embedded in the anode chamber for a certain reaction time. The reactor temperature was controlled at 50 °C. All electrochemical data was collected vs. a  $\text{Hg/HgO}/1.0 \text{ M KOH}$  reference electrode and converted to a reversible hydrogen electrode (RHE) by  $V_{\text{vs. RHE}} = V_{\text{measured vs. Hg/HgO/1.0 M KOH}} + 0.098 + 0.059 \times (\text{pH of electrolyte solution})$ .

### 2.5. Electro-oxidation of glycerol in half cell with in-situ sample collection

The half cell in-situ sample collection test was conducted at room temperature in a conventional three-electrode-cell setup following the procedure in our previous work [27]. Briefly, 2.0 mg of the as-prepared Au/C catalyst were dispersed in 1.0 ml isopropanol by sonication to form a uniform ink. The working electrode was prepared by drop-casting 40  $\mu\text{l}$  of the ink onto the glassy carbon electrode. 20  $\mu\text{l}$  of 0.05 wt% AS-4 anion conductive ionomer solution (Tokuyama Inc. Japan) was then added on the top to affix the catalyst. A  $\text{Hg/HgO}/1.0 \text{ M KOH}$  and a Pt wire were applied as the reference and counter electrodes, respectively. The electrochemical data was also reported versus RHE. A linear staircase scan in  $\text{N}_2$ -saturated 0.1 M KOH + 0.1 M glycerol was carried out with the increment of 100 mV 10 min $^{-1}$ . In the course of the voltammetry, the products under each potential were in-situ collected through a needle positioned within 0.5 mm to the center of working electrode surface.

### 2.6. Products analyses

The oxidation products were analyzed by high-performance liquid chromatography (HPLC, Agilent 1100), with a refractive index detector (RID, Agilent G1362A) and a variable wavelength detector (VWD, 220 nm, Agilent G1314A). An OA-1000 column (Alltech) operated at 60 °C, and an eluent of 5 mM aqueous sulfuric acid flowing at 0.3 ml min<sup>-1</sup> were applied for the product separation. 20 µl of sample was injected into the HPLC system. Products were identified by comparison with authentic samples.

The product selectivity is calculated as:

$$\text{Selectivity} = \frac{\text{Moles of specific product forms}}{\text{Total moles of C}_2 \text{ and C}_3 \text{ products detected}} \times 100\% \quad (1)$$

The carbon balance is based on:

$$\text{Carbon balance} = \frac{3M_{G_i} - 3M_{C_3} - 2M_{C_2} - M_{C_1} - 3M_{G_f}}{3M_{G_i}} \times 100\% \quad (2)$$

If assuming that no C<sub>2</sub> products were further oxidized to C<sub>1</sub> products, then,

$$M_{C_2} = M_{C_1} \quad (3)$$

Therefore:

$$\text{Carbon balance} = \frac{M_{G_i} - M_{C_3} - M_{C_2} - M_{G_f}}{M_{G_i}} \times 100\% \quad (4)$$

where M<sub>G<sub>i</sub></sub> and M<sub>G<sub>f</sub></sub> are the initial and final moles of glycerol in the electrolyte, and , , and are the moles of C<sub>3</sub> products (glycerate, tartronate and mesoxalate), C<sub>2</sub> products (glycolate, glyoxylate and oxalate), and C<sub>1</sub> products (formate and carbonate), respectively. A smaller carbon balance value indicates less C<sub>2</sub> intermediates were further oxidized to C<sub>1</sub> products. A carbon balance of 0 means all the C<sub>2</sub> products generated from C-C breaking of C<sub>3</sub> products do not undergo further C-C cleavage, and summation of the moles of all the C<sub>2</sub> and C<sub>3</sub> products and unreacted glycerol is equal to moles of the initial glycerol. The carbon balance under all the tests condition is less than 10%, which is within the system error expected in HPLC analysis.

## 3. Results and discussion

The XRD pattern of the Au/C catalyst was collected from 15° to 100°, and displays a typical face-center cubic (FCC) pattern (JCPDS card 4-784) in Fig. 1. The diffraction peaks at 38.4°, 44.2°, 64.7°, 77.9°, and 81.4° are assigned to Au (111), (200), (220), (311), and (222), respectively, while that at 25.0° is referred to the graphite (002) of the carbon support. The average Au crystal size calculated based on the Au (220) diffraction peak is 3.4 nm, using the Debye–Scherrer formula as shown below [33]:

$$L = \frac{0.9\lambda_K\alpha}{B_{2\theta} \cos\theta_{\max}} \quad (5)$$

where L is the mean crystal size,  $\lambda$  is the wavelength of the x-ray (1.5406 Å), B is the full width at half-maximum of the peak (rad) and  $\theta_{\max}$  is the Bragg angle (rad) of Au (220).

A typical TEM image and HR-TEM image of Au/C are shown in Fig. 2a and b, and clearly evidenced that most Au-NPs are uniformly dispersed on the carbon support with an average particle size of 3.5 nm. The histogram of particle sizes in Fig. 2c was evaluated from over 100 particles in arbitrarily chosen areas, and suggests a narrow size distribution of 2–6 nm.

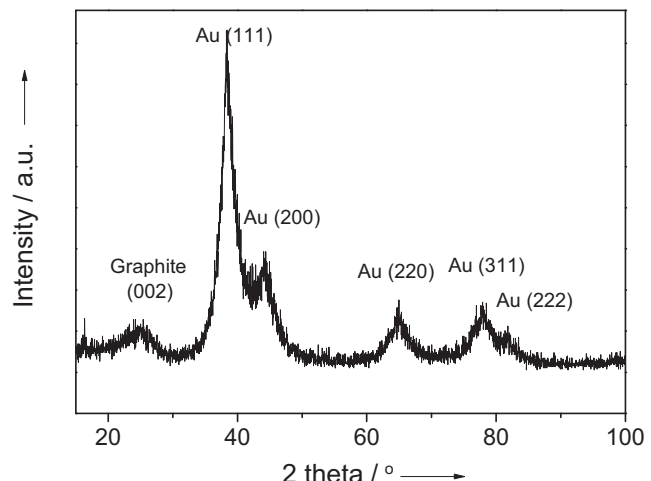


**Fig. 1.** XRD patterns of Au/C catalyst (40 wt%).

The potential-tuned oxidation of glycerol was investigated in an electro-catalytic flow reactor illustrated in Fig. 3. A Teflon-untreated carbon cloth was employed as the liquid fuel diffusion layer and the conductive substrate. A volume of 8 ml 2.0 M KOH + 1.0 M glycerol solution was continuously looped from the fuel vessel into the anode, and was allowed to react at 50 °C under a certain applied potential. The glycerol electro-oxidation current as a function of time at each applied potential is shown in Fig. 4. It can be observed that the current at most potentials remains stable over the course of test (1 h), indicating little deactivation or loss of Au catalyst. However, a slight but noticeable current drop observed at the most positive potentials, 0.65 and 0.7 V vs. RHE tested could result from the faster reaction rates which give rise to the more serious mass transport issue, in particularly at the cathode side where hydrogen evolution reaction occurs, as the bubbles will block the active area of the Pt/C based liquid diffusion electrode from contacting fresh electrolytes.

The product distributions under different applied potentials after 1 h at 50 °C were summarized in Fig. 5. It clearly demonstrated that the selectivity to each product was strongly regulated by anode potential. At potentials <0.45 V, the main product was tartronate, with the selectivity of >79%, while no mesoxalate was observed. Mesoxalate generation was observed at the potentials ≥0.45 V. Its selectivity ramped up gradually by increasing the applied potentials, and reached the maximum selectivity of 57% at 0.65 V. Meanwhile, the selectivity to tartronate concomitantly decreased to 26% (at 0.65 V). The trend strongly suggests a potential controlled conversion from tartronate to mesoxalate, which takes place ≥0.45 V, and is further enhanced at higher potentials. When further increasing the anode applied potential to 0.7 V, the selectivity to mesoxalate decreased to 55%, while the selectivity to oxalate increased from 5% (at 0.65 V) to 8%, indicating some mesoxalate was over-oxidized to oxalate.

It has been reported that in a three-electrode half cell system with a polycrystalline Au electrode, the only glycerol oxidation product in alkaline media is glycerate, at low potentials ( $\leq 0.8$  V) [14,24]. However, in the carbon cloth based electro-catalytic flow reactor, the main products are tartronate and mesoxalate at potentials  $\leq 0.7$  V. As shown in Eqs. (6)–(8), the thermodynamic potentials of glycerol oxidation to glycerate, tartronate, and mesoxalate at standard conditions are −0.74 V, −0.77 V and −0.72 V vs. SHE in a basic electrolyte with pH of 14 (thermodynamic properties of some biomass compounds are obtained from reference [34]), which are very close to each other. Thermodynamically, it is possible to obtain these products simultaneously. The difference between

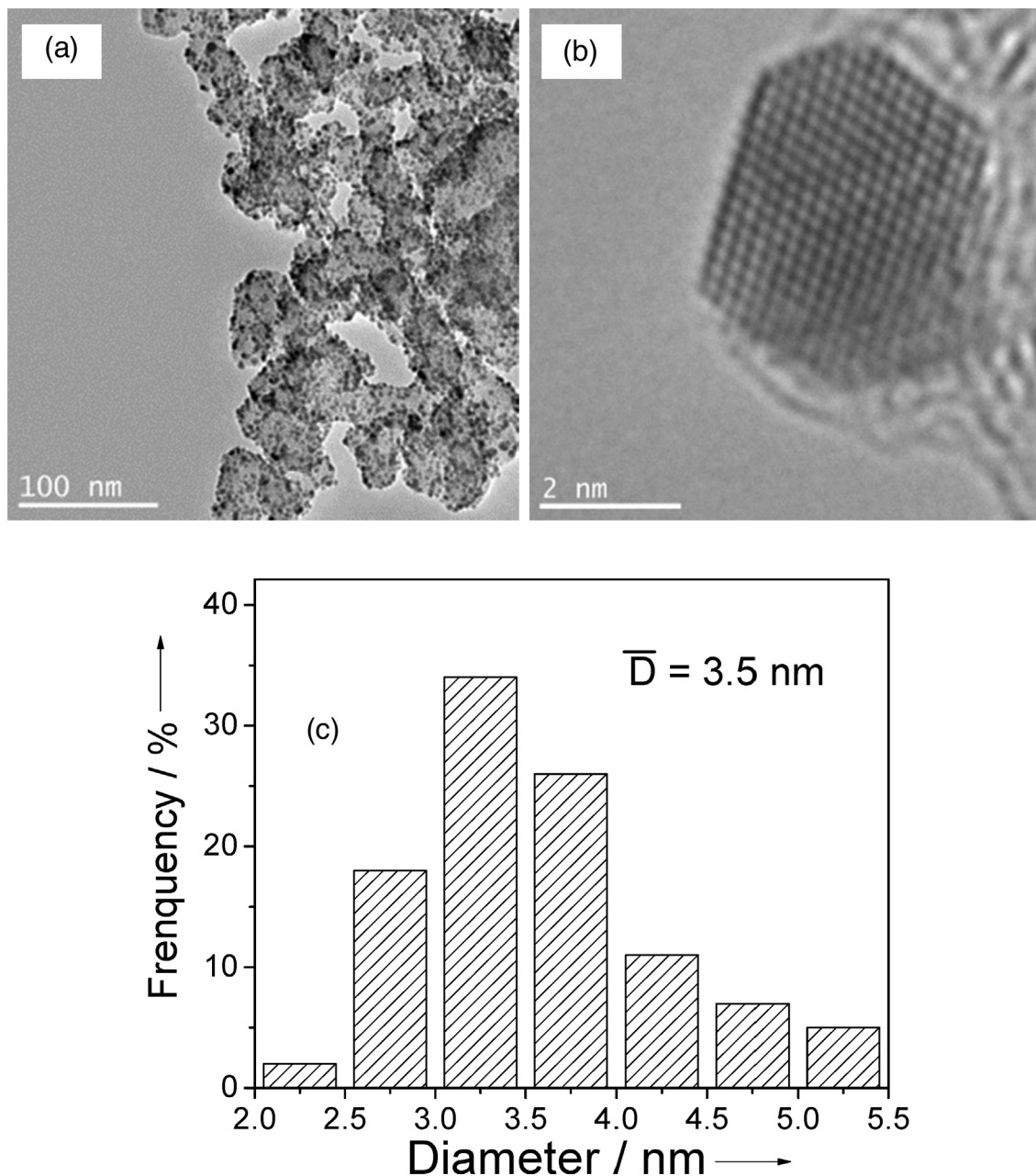


**Fig. 2.** TEM (a) and HR-TEM (b) images and histogram (c) of Au/C catalyst (40 wt%).

product distributions in these two systems therefore lies in the different electrode structures, which can significantly influence reactant transport/diffusion (to catalyst surface), and therefore affect the overall reaction kinetics. In the course of glycerol oxidation, glycerate is the first stable product, as well as a reaction 'intermediate' required for the production of tartronate. When the flat surface Au electrode was employed, the generated glycerate would irreversibly diffuse from the electrode surface to the bulk electrolyte, which will prevent the further oxidation process. In the electro-catalytic flow reactor, the carbon cloth can work as a porous matrix that helps holding/trapping the stable reaction 'intermediates' (glycerate, tartronate, etc.) from escaping, thus the final oxidation product generation could be better controlled by the electrode potential, as demonstrated in this paper.



$$E^\circ = -0.74 \text{ V vs. SHE} \quad (6)$$



$$E^\circ = -0.77 \text{ V vs. SHE} \quad (7)$$



$$E^\circ = -0.72 \text{ V vs. SHE} \quad (8)$$

In order to bridge the differences between the three-electrode half cell and the carbon cloth based electro-catalytic flow reactor, a thin layer of Au/C was dropcasted on a glassy carbon disk and served as the working electrode, and glycerol electro-oxidation was tested with our self-assembled in-situ sample collection ex-situ HPLC analysis technique in a three-electrode cell [27,35] using a staircase linear voltammetry. The polarization curve and the products concentration profile are summarized in Fig. 6. Due to a lower temperature ( $25^\circ\text{C}$  vs.  $50^\circ\text{C}$ ) lower Au catalyst loading ( $163 \mu\text{g cm}^{-2}$  vs.  $5 \text{ mg cm}^{-2}$ ) and fuel concentration ( $0.1 \text{ M KOH} + 0.1 \text{ M Glycerol}$

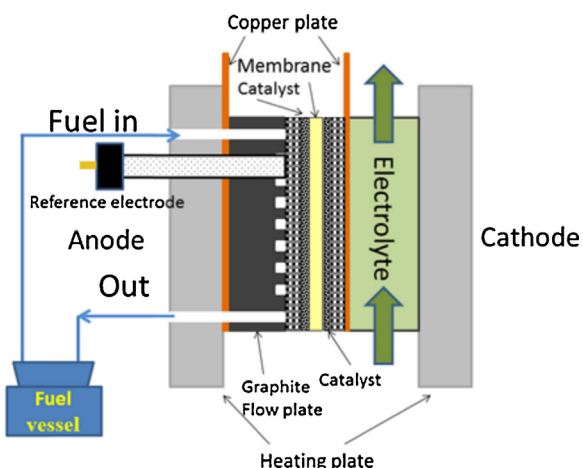


**Fig. 3.** Schematic illustration of the anion-exchange membrane-based electro-catalytic flow reactors.

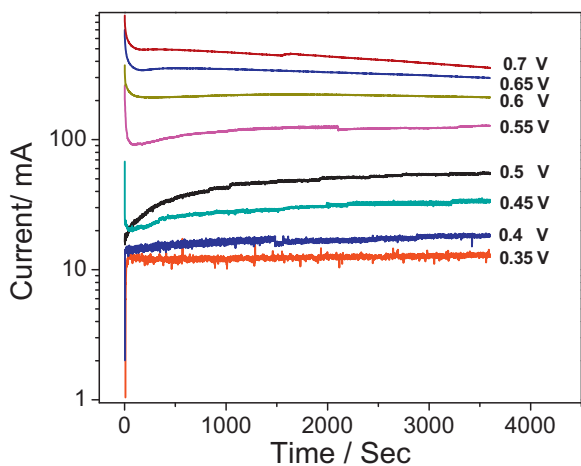


**Fig. 4.** Glycerol electro-oxidation current as a function of time at different potentials (V vs. RHE).

vs. 2.0 M KOH + 1.0 M Glycerol), the onset potential observed in the three-electrode system (0.7 V vs. RHE) is more positive than the one obtained in the AEM electro-catalytic flow reactor (0.25 V vs. RHE) (Fig. S1 in [Appendix A](#)). It has also been reported that the electro-oxidation of glycerol on polycrystalline Au electrode will only generate glycerate and glycolate [14,24]. However, when

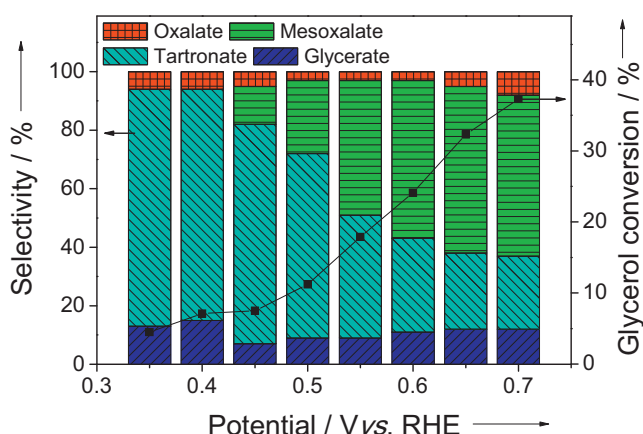


**Fig. 5.** Electro-oxidation of glycerol (2.0 M KOH + 1.0 M glycerol) on Au/C under different applied potentials, 1 h, 50 °C.

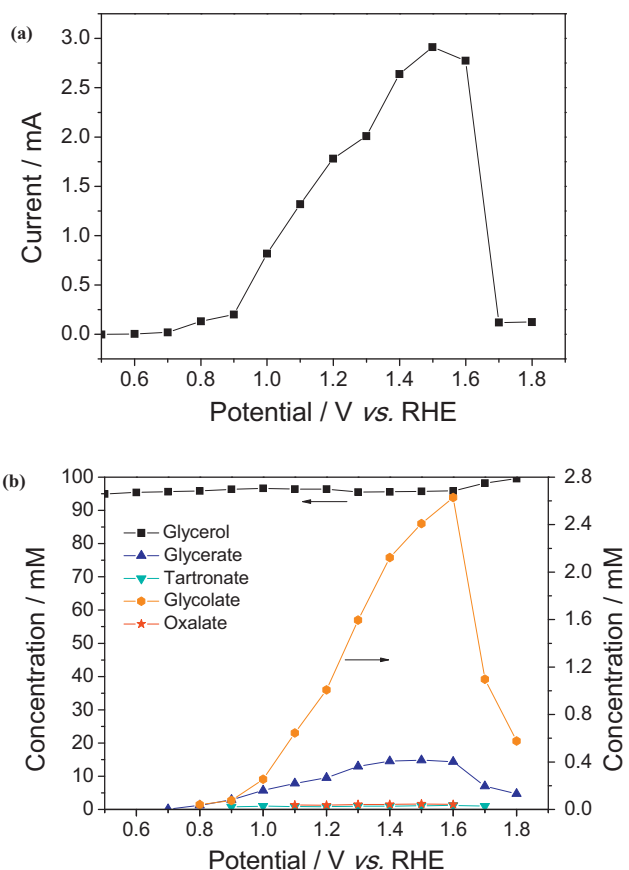


**Fig. 6.** Electro-oxidation of glycerol on Au/C thin layer electrode: (a) polarization curve and (b) oxidation products concentration profile in 0.1 M KOH + 0.1 M glycerol.

using the thin layer Au/C catalyst as the electrode, the Au/C particles are randomly packed on the glassy carbon and form a thin porous matrix, which will help retain glycerate in the catalyst layer. As a result, beside the main products of glycerate and glycolate, trace amount of tartronate was detected during the staircase linear voltammetry. However, due to poor “holding effect” of the thin porous layer (usually <3 μm, detailed calculation is shown in [Appendix A](#), Table S1), the trace amount of tartronate was only observed at higher potentials (>0.9 V), at which the overall glycerol oxidation rate to tartronate is enhanced. Therefore, in order to achieve reasonable production quantity of tartronate and its further oxidation product mesoxalate, a real porous liquid diffusion electrode (thickness >700 μm, consisting of carbon cloth substrate: 381 μm and catalyst layer: 324 μm, measured by micrometer) with a confined electrolyte volume (as in the presented electro-catalytic flow reactor, [Fig. 3](#)) is needed and used in this study.

To further confirm the dominant effect of anode potential over glycerol electro-oxidation, we held the reaction temperate at 50 °C and elongated the reaction time at both the lower and higher anode potentials of 0.4 V and 0.65 V. As shown in [Fig. 7\(a\)](#), by applying an anode potential of 0.4 V, the glycerol conversion continuously increased with the elongation of reaction time and reached 35% after 18 h. However, the selectivity to tartronate remained stable at ~78%, which implies that the selectivity to tartronate is mainly controlled by the applied potential, and is weakly influenced by the reaction time. The selectivity to oxalate slightly increased for a longer reaction time, possibly due to the slow oxidation of tartronate to glyoxylate, which is then quickly oxidized to oxalate. No mesoxalate was observed even after 18 h of reaction, indicating that the oxidation from tartronate to mesoxalate was firmly regulated by the anode potential, and can only take place at

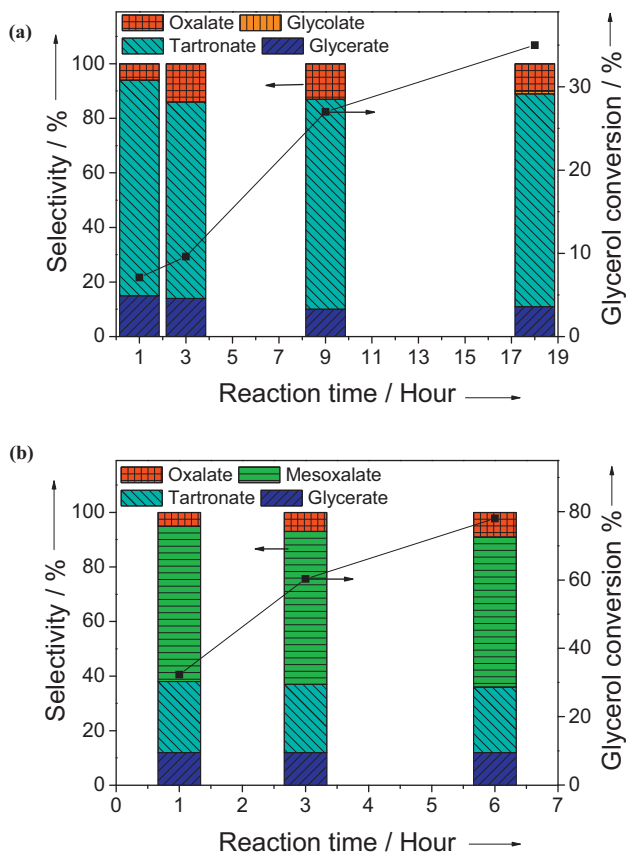


**Fig. 7.** Electro-oxidation of glycerol (2.0 M KOH + 1.0 M glycerol) on Au/C at (a) 0.4 V vs. RHE and (b) 0.65 V vs. RHE at 50 °C for different reaction time.

potentials higher than 0.45 V at this specific condition. It is noted that a trace amount of glycolate was observed (<1%) after the 18 h reaction. Although glycolic acid can be formed from tartaric acid through a non-Faradic decarboxylation process in a non-oxidizing, low pH environment [36], it is not favored on polarized Au catalysts in an alkaline electrolyte [19]. Therefore, the observation of a small amount of glycolate at long reaction times indicates that an oxidation of glycerate to glycolate takes place very slowly at this low applied potential through C–C bond cleavage. As reported in our previous publication, when the anode applied potential is further increased to 1.6 V, the C–C bond breaking can become predominant, which leads to a high selectivity to glycolate [37].

The potential-regulation effect was also confirmed at a higher potential of 0.65 V (Fig. 7b). Fed with 2.0 M KOH + 1.0 M glycerol, the selectivities to tartronate and mesoxalate after 1 h of reaction were 26% and 57%, respectively, while the conversion of glycerol was 32%. When the reaction time was increased to 6 h, the selectivities to tartronate and mesoxalate only slightly decreased to 24% and 55%, respectively, while glycerol conversion was increased to 78%. This strongly indicates that the selectivities to the main products, tartronate and mesoxalate, are controlled by the anode potential, and is only weakly affected by the reaction time or glycerol conversion. The slight decrease in tartronate and mesoxalate selectivities is probably due to the over-oxidation to oxalate, which can be outlined by the increasing of the selectivity to the byproduct oxalate from 5% (after 1 h) to 9% (after 6 h).

The KOH to glycerol ratio is a critical parameter for glycerol oxidation [27,37,38], here the electro-oxidation of glycerol was investigated with different initial glycerol concentrations, while fixing the KOH concentration at 2.0 M. The results in Fig. 8 show

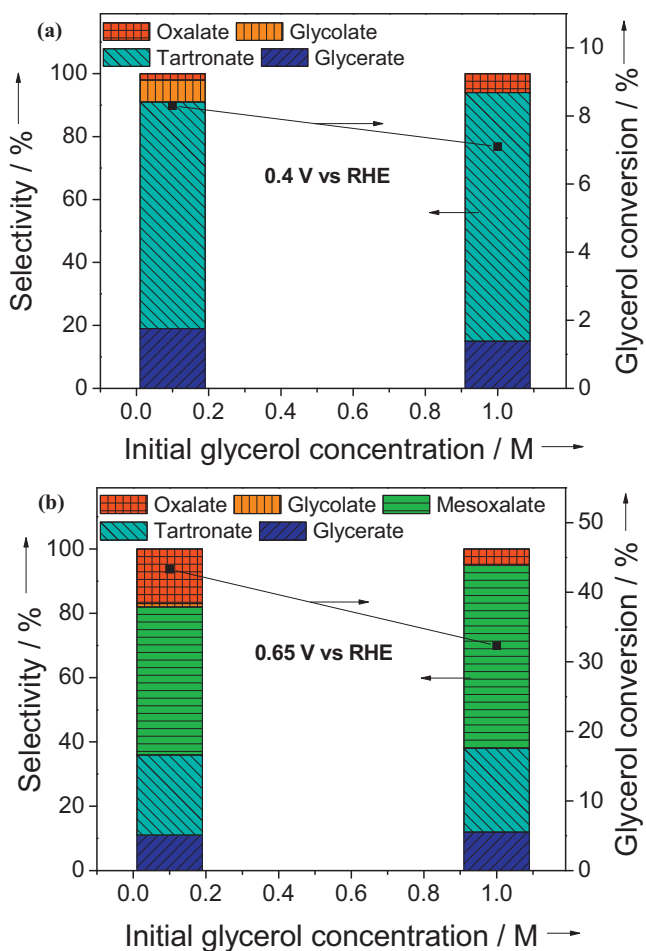
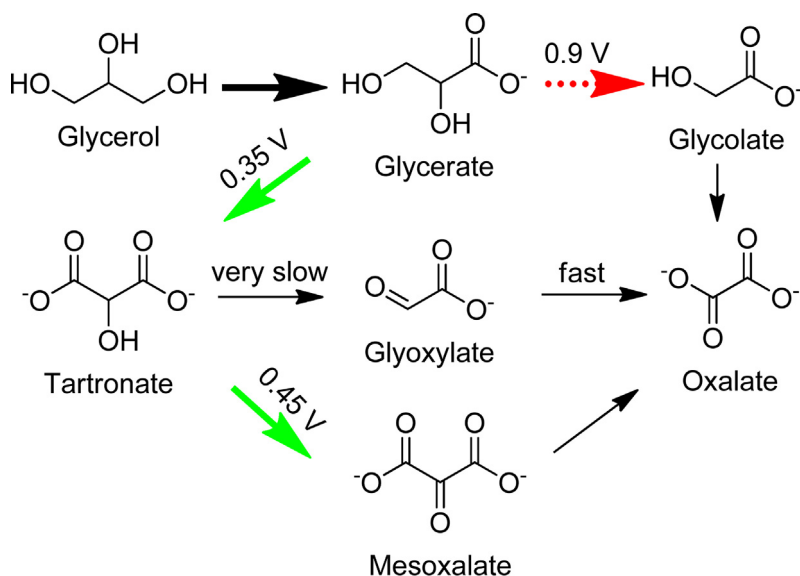


**Fig. 8.** KOH: glycerol ratio effects at the applied potential of (a) 0.4 V vs. RHE and (b) 0.65 V vs. RHE, for 1 h, 50 °C, [KOH]: 2.0 M.

that a higher ratio of KOH to glycerol concentration will increase the selectivity to C<sub>2</sub> products (glycolate or oxalate). At the anode potential of 0.4 V (Fig. 8a), a selectivity of 7% to glycolate was observed after 1 h of reaction in 2.0 M KOH + 0.1 M glycerol. However, when 2.0 M KOH + 1.0 M glycerol was used, only <1% of glycolate was detected even after 18 h of reaction (Fig. 7a). This indicates that a lower glycerol initial concentration will facilitate the oxidation of glycerate to glycolate. The facilitation from glycerate to glycolate at lower glycerol initial concentrations was also confirmed in our previous work at high potentials where the C–C bond cleavage is the dominant reaction [37]. At the applied potential of 1.6 V, the selectivity to glycolate on Au/CNT catalyst increased from 78% to 87%, when the initial glycerol concentration decreased from 2.0 M to 0.5 M. The KOH: glycerol ratio effect was also investigated at the anode potential of 0.65 V, at which there was the highest selectivity to mesoxalate after 1 h of reaction. When the initial glycerol concentration was reduced from 1.0 to 0.1 M (Fig. 8b), the selectivity to oxalate increased from 5% to 17%, while that to mesoxalate decreased from 57% to 46%, indicating the oxidation of mesoxalate to oxalate was enhanced at a lower initial glycerol concentration. In addition, a trace amount of glycolate was also observed, due to the enhanced oxidation rate of glycerate to glycolate at the lower initial glycerol concentration.

Based on the experimental observations, a reaction path of glycerol electro-oxidation on Au/C catalyst at 50 °C was summarized in Fig. 9. Glycerol is first oxidized to glycerate, which is observed starting from 0.35 V. It is noted that the selectivity to glycerate is stabilized at 10–20%, and is almost not affected by the



**Bold arrows:** main reactions; **Normal arrows:** minor reactions;

**Green:** favored at lower potentials; **Red dashed:** favored at higher potentials

\*C<sub>1</sub> products are not included in the scheme; switch potentials are marked vs. RHE.

**Fig. 9.** Proposed reaction path for electro-oxidation of glycerol (2.0 M KOH + 1.0 M glycerol) on Au/C at 50 °C. The switch potentials were obtained under the reported operation conditions based on the presented anode structures.

anode potential or reaction time. This indicates that the selectivity to glycerate in the electro-catalytic flow reactor is probably controlled by diffusion. Glycerol first diffuses from the bulk electrolyte into the catalyst layer and is oxidized to glycerate. While some glycerate dissolves from the catalyst layer into the bulk electrolyte, most of it is still “trapped” in the thick catalyst layer due to the high Au loading (5.0 mg cm<sup>-2</sup>), and the adsorbed glycerate is further oxidized through either the oxidation of second primary alcohol group or the C-C bond breakage. The percentage of glycerate dissolved into the bulk electrolyte is mainly controlled by the diffusion in the system. When desorbed from catalyst surface and dissolved into the bulk electrolyte, glycerate seems hard to further react on the Au catalyst. As a result, the selectivity to glycerate is always stable and independent of applied potential or reaction time. In the present work of glycerol electro-oxidation at lower potentials, the adsorbed glycerate on Au surface is then quickly oxidized to tartronate (the green arrow pathway in Fig. 9). Due to the similar structure of the two primary alcohol groups in glycerol, it is reasonable to believe the activation energies for their oxidation are close and require a similar overpotential to produce both glycerate and tartronate in the electro-catalytic process. Therefore, tartronate is also observed from 0.35 V. The adsorbed glycerate is also oxidized to glycolate through a C-C bond breakage reaction. This step is very slow at lower applied potentials (i.e.  $\leq 0.9$  V). It needs to mention that at higher applied potentials, the C-C bond breakage reaction is greatly accelerated even at room temperature, leading to a high selectivity to glycolate [37]. Comparing to the oxidation of glycerate to tartronate, the oxidation of the alcohol group in tartronate (secondary alcohol group in glycerol) is more potential-sensitive, which requires a higher anode potential of  $\geq 0.45$  V at 50 °C. The oxidation rate of the adsorbed tartronate to mesoxalate is improved when the anode applied potential is further increased, which is evidenced by the continuously increasing of the mesoxalate selectivity and the corresponding decrease in tartronate selectivity. Simoes et al. reported on Au catalysts, the infrared spectra indicates glycerol is first oxidized to hydroxypyruvate at 0.7 V, which may be further oxidized to mesoxalate [20]. However, in our work, no detectable hydroxypyruvate was

observed under any investigated potentials, indicating that mesoxalate should be generated through the tartronate pathway under the taken oxidation conditions in the AEM electro-catalytic flow reactor. Mesoxalate is slowly over-oxidized to oxalate, leading to a slight increase in the selectivity to oxalate at a longer reaction time. At lower applied potentials of  $< 0.4$  V, the adsorbed tartronate could also be oxidized to glyoxylate, which is then quickly oxidized to oxalate, therefore, oxalate was observed without observation of any glyoxylate. As shown in the reaction path roadmap, at lower applied potentials ( $\leq 0.9$  V), the C<sub>2</sub> product oxalate might be mainly generated from over-oxidation of tartronate and mesoxalate.

#### 4. Conclusions

In this work, we demonstrated an efficient controllable electro-catalytic process based on an Au/C catalyst and glycerol system. The oxidation of glycerol can be tuned by anode potential to produce tartronate (oxidizing two primary -OH,  $\geq 0.35$  V), mesoxalate (oxidizing three -OH,  $\geq 0.45$  V), or glycolate (breaking C-C bond,  $> 0.9$  V). This study opens a new strategy for the targeted transformation of biomass compounds with poly-alcohol or multi-functional groups into valuable chemicals.

#### Acknowledgements

We acknowledge the US National Science Foundation (CBET-1159448) for funding. Acknowledgment is also made to the Research Excellence Fund-Research Seeds (REF-RS) grant (E49290) from Michigan Tech for partial support of this research. Le Xin thanks a Michigan Tech Doctoral Finishing Fellowship and Ji Qi is grateful to the financial support from the Chinese Scholarship Council.

#### Appendix A. Supplementary data

Supplementary data associated with this article can be found, in the online version, at <http://dx.doi.org/10.1016/j.apcatb.2013.10.018>.

## References

- [1] P. Gallezot, Chemical Society Reviews 41 (2012) 1538–1558.
- [2] B.O. Palsson, S. Fathi-Afshar, D.F. Rudd, E.N. Lightfoot, Science 213 (1981) 513–517.
- [3] Biomass Research and Development Technical Advisory Committee, Road Map for Bioenergy and Biobased Products in the United States, 2007.
- [4] J.J. Bozell, G.R. Petersen, Green Chemistry 12 (2010) 539–554.
- [5] A. Corma, S. Iborra, A. Velty, Chemical Reviews 107 (2007) 2411–2502.
- [6] J.N. Chheda, G.W. Huber, J.A. Dumesic, Angewandte Chemie International Edition 46 (2007) 7164–7183.
- [7] B. Katryniok, H. Kimura, E. Skrzynska, J.-S. Girardon, P. Fongarland, M. Capron, R. Ducoulombier, N. Mimura, S. Paul, F. Dumeignil, Green Chemistry 13 (2011) 1960–1979.
- [8] N. Dimitratos, J.A. Lopez-Sanchez, G.J. Hutchings, Topics in Catalysis 52 (2009) 258–268.
- [9] C.H.C. Zhou, J.N. Beltramini, Y.X. Fan, G.Q.M. Lu, Chemical Society Reviews 37 (2008) 527–549.
- [10] S. Carrettin, P. McMorn, P. Johnston, K. Griffin, G.J. Hutchings, Chemical Communications (2002) 696–697.
- [11] M. Pagliaro, R. Ciriminna, H. Kimura, M. Rossi, C. Della Pina, Angewandte Chemie International Edition 46 (2007) 4434–4440.
- [12] G.L. Brett, Q. He, C. Hammond, P.J. Miedziak, N. Dimitratos, M. Sankar, A.A. Herzing, M. Conte, J.A. Lopez-Sanchez, C.J. Kiely, D.W. Knight, S.H. Taylor, G.J. Hutchings, Angewandte Chemie International Edition 50 (2011) 10136–10139.
- [13] Y. Kwon, Y. Birdja, I. Spanos, P. Rodriguez, M.T.M. Koper, ACS Catalysis 2 (2012) 759–764.
- [14] Y. Kwon, M.T.M. Koper, Analytical Chemistry 82 (2010) 5420–5424.
- [15] B.N. Zope, D.D. Hibbitts, M. Neurock, R.J. Davis, Science 330 (2010) 74–78.
- [16] A. Villa, G.M. Veith, L. Prati, Angewandte Chemie International Edition 49 (2010) 4499–4502.
- [17] H. Kimura, JP1994315623, Kao Corp, Japan, 1996.
- [18] P. Gallezot, Catalysis Today 37 (1997) 405–418.
- [19] H. Kimura, T. Imanaka, Y. Kokota, JP199395253, Kao Corp, Japan, 1994.
- [20] M. Simoes, S. Baranton, C. Coutanceau, Applied Catalysis B: Environmental 93 (2010) 354–362.
- [21] M. Simões, S. Baranton, C. Coutanceau, Applied Catalysis B: Environmental 110 (2011) 40–49.
- [22] M. Mougenot, A. Caillard, M. Simoes, S. Baranton, C. Coutanceau, P. Brault, Applied Catalysis B: Environmental 107 (2011) 372–379.
- [23] L. Roquet, E.M. Belgisir, J.M. Leger, C. Lamy, Electrochimica Acta 39 (1994) 2387–2394.
- [24] Y. Kwon, K.J.P. Schouten, M.T.M. Koper, ChemCatChem 3 (2011) 1176–1185.
- [25] M. Simões, S. Baranton, C. Coutanceau, ChemSusChem 5 (2012) 2106–2124.
- [26] J. Gomes, G. Tremiliosi-Filho, Electrocatalysis 2 (2011) 96–105.
- [27] Z. Zhang, L. Xin, W. Li, Applied Catalysis B: Environmental 119–120 (2012) 40–48.
- [28] L. Xin, Z. Zhang, Z. Wang, W. Li, ChemCatChem 4 (2012) 1105–1114.
- [29] V. Bambagioni, C. Bianchini, A. Marchionni, J. Filippi, F. Vizza, J. Teddy, P. Serp, M. Zhiani, Journal of Power Sources 190 (2009) 241–251.
- [30] A. Marchionni, M. Bevilacqua, C. Bianchini, Y.-X. Chen, J. Filippi, P. Fornasiero, A. Lavacchi, H. Miller, L. Wang, F. Vizza, ChemSusChem 6 (2013) 518–528.
- [31] Z. Zhang, L. Xin, W. Li, International Journal of Hydrogen Energy 37 (2012) 9393–9401.
- [32] Z. Zhang, L. Xin, J. Qi, D.J. Chadderton, W. Li, Applied Catalysis B: Environmental 136–137 (2013) 29–39.
- [33] O. Winjobi, Z. Zhang, C. Liang, W. Li, Electrochimica Acta 55 (2010) 4217–4221.
- [34] M. Vasiliu, K. Guynn, D.A. Dixon, Journal of Physical Chemistry C 115 (2011) 15686–15702.
- [35] L. Xin, Z. Zhang, J. Qi, D. Chadderton, W. Li, Applied Catalysis B: Environmental 125 (2012) 85–94.
- [36] M. Sankar, N. Dimitratos, D.W. Knight, A.F. Carley, R. Tiruvalam, C.J. Kiely, D. Thomas, G.J. Hutchings, ChemSusChem 2 (2009) 1145–1151.
- [37] Z. Zhang, L. Xin, J. Qi, Z. Wang, W. Li, Green Chemistry 14 (2012) 2150–2152.
- [38] J. Qi, L. Xin, Z. Zhang, K. Sun, H. He, F. Wang, D. Chadderton, Y. Qiu, C. Liang, W. Li, Green Chemistry 15 (2013) 1133–1137.